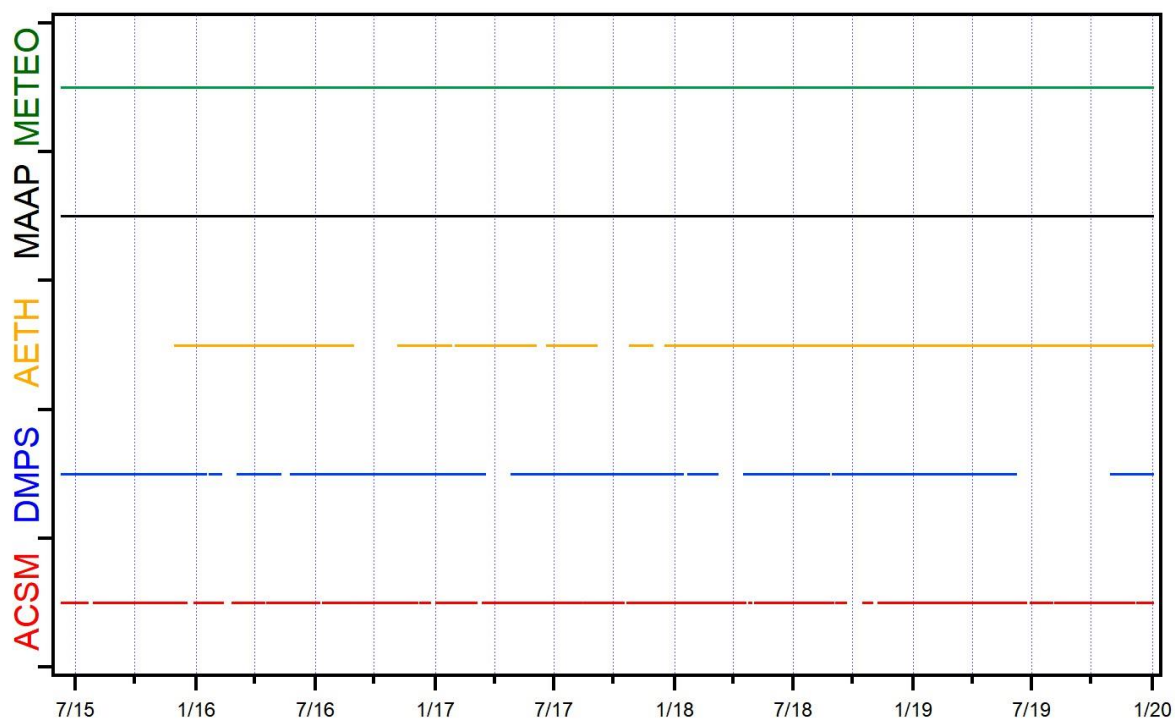


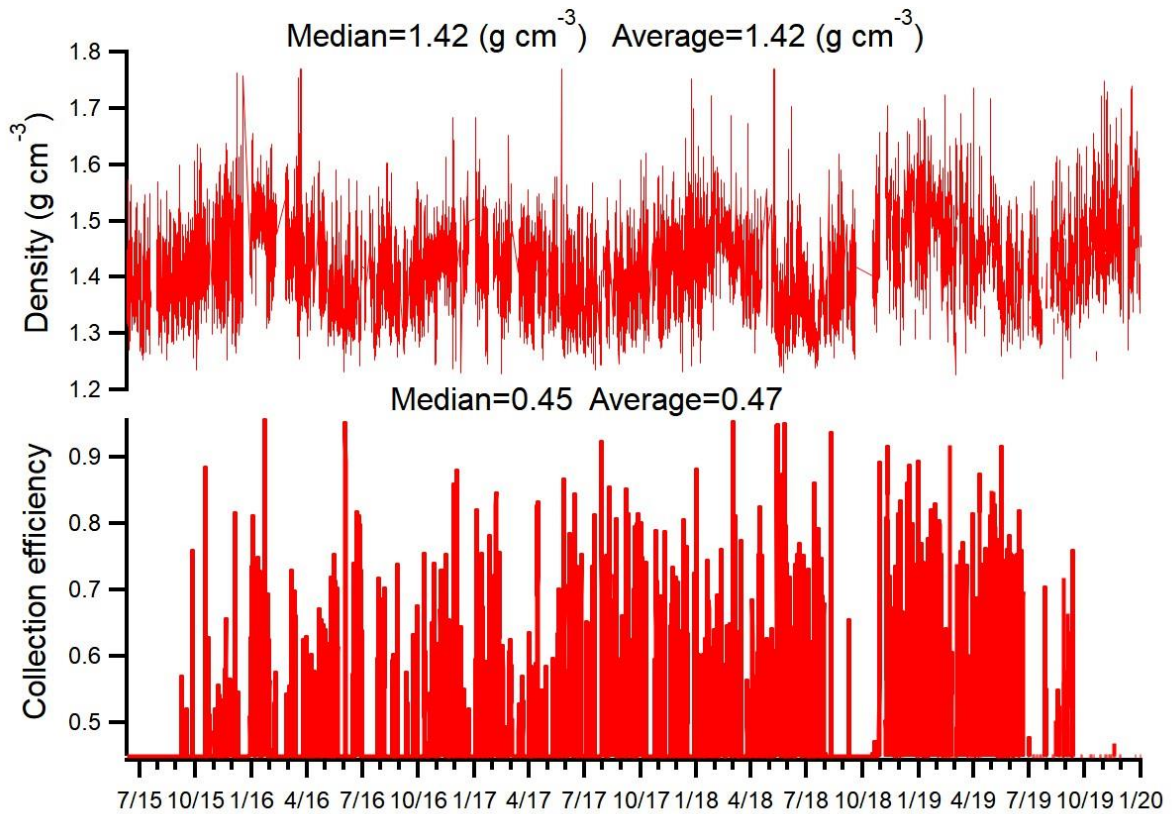
1 S1 Supplemental graphics and results



2

3 Figure S1: Measurement periods of instruments employed in this study.

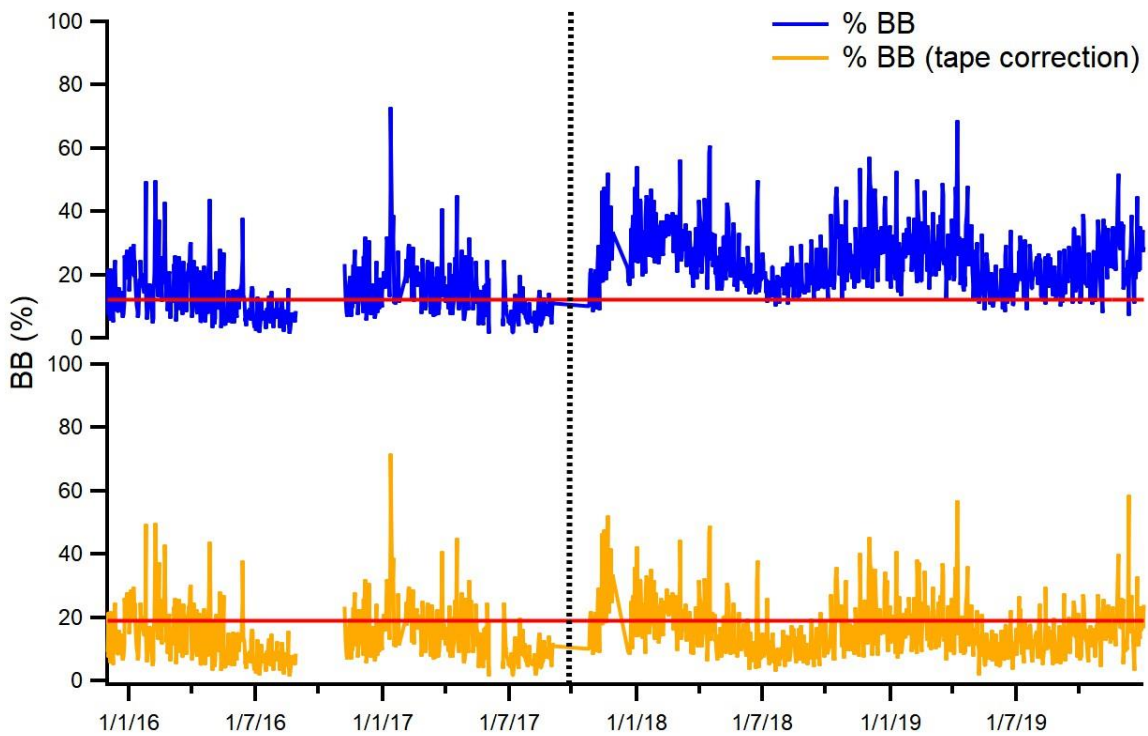
4



5

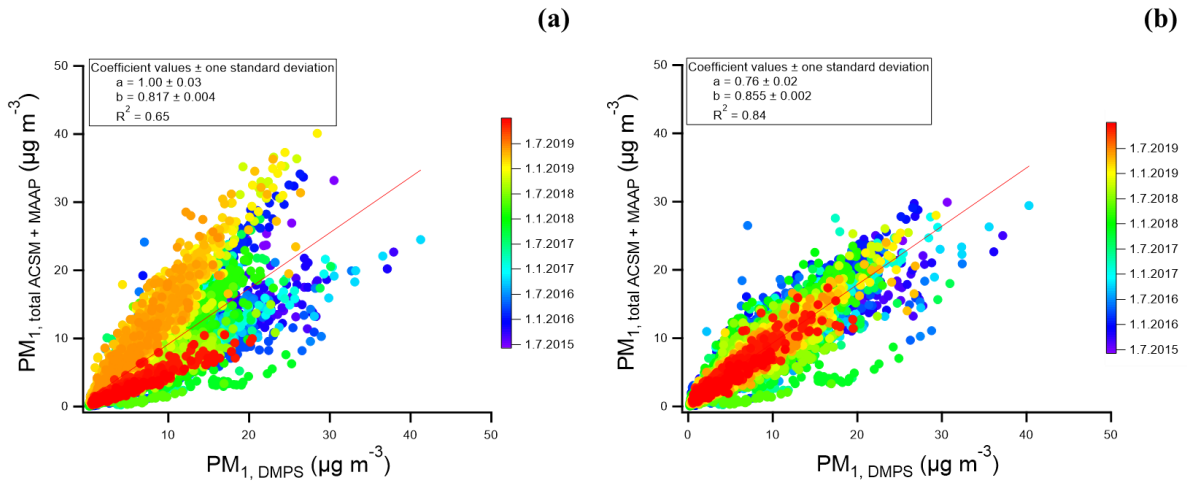
6 **Figure S2: Density (top plot) and collection efficiency (bottom plot) determined during this study. Median and average**
 7 **values were included in the graphic.**

8



9
10
11
12

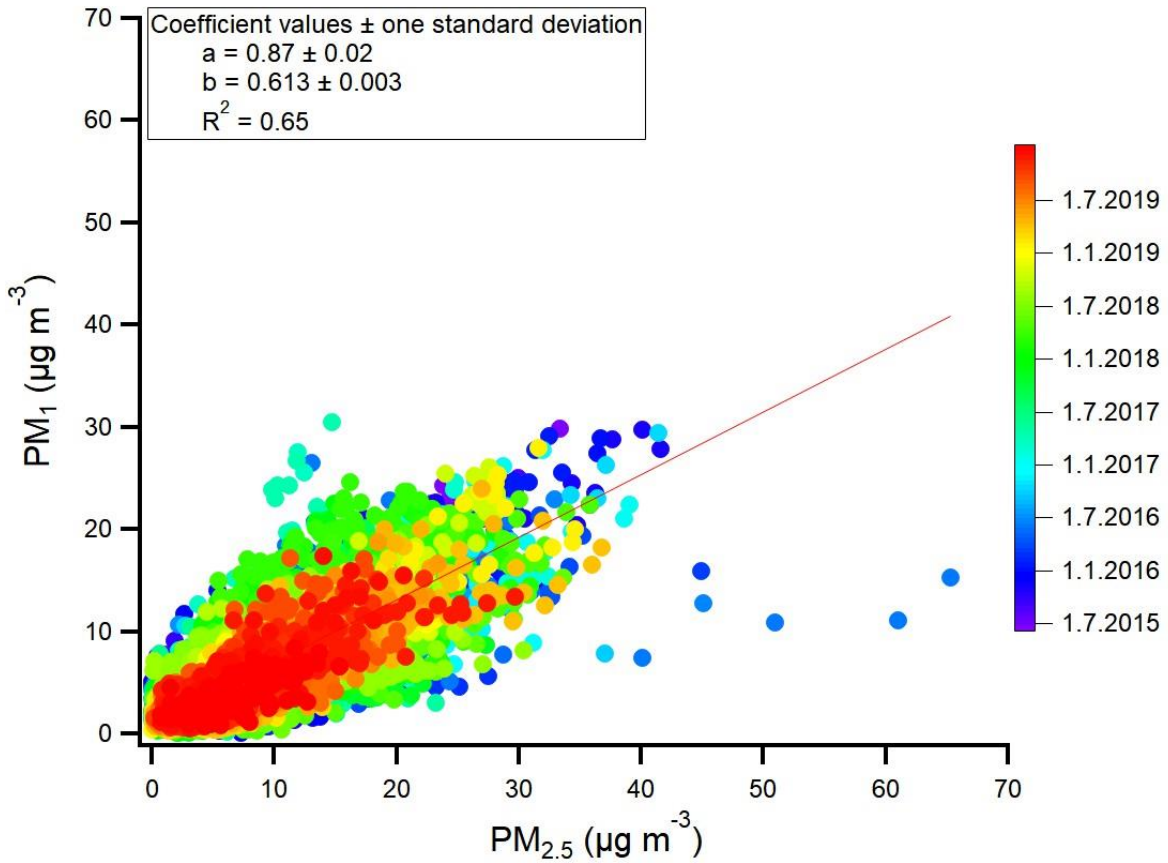
Figure S3: Correction applied to biomass burning (BB) percentage due to a change in the type of filter tape used during
measurements. The red lines are the mean BB before correction (top plot) and during the entire period (bottom plot),
while black line indicates the period after which the correction was applied.



13

14
15
16
17

Figure S4: Total ACSM concentrations plus eBC measured by MAAP vs. PM₁ measured by DMPS, coloured according to the sampling time, before (a) and after (b) the employed correction. Slope coefficients and corresponding standard deviations were included.

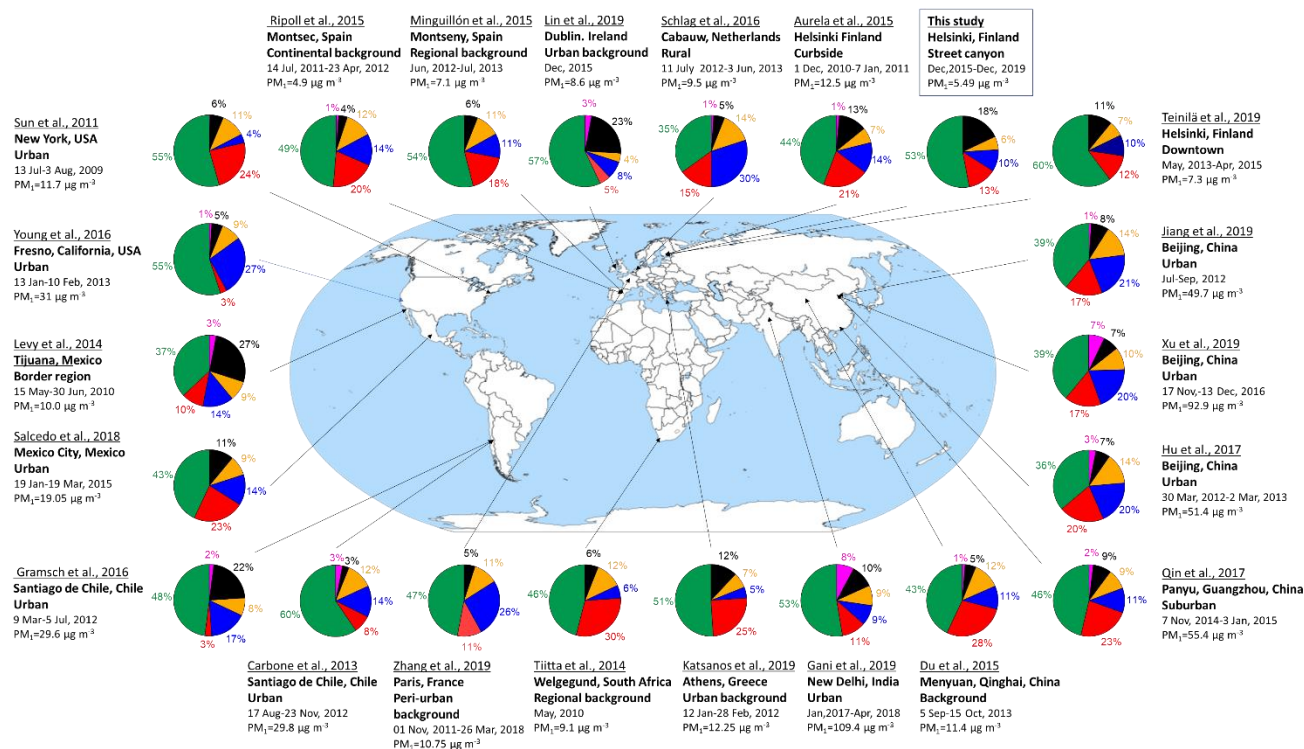


18

19
20
21
22

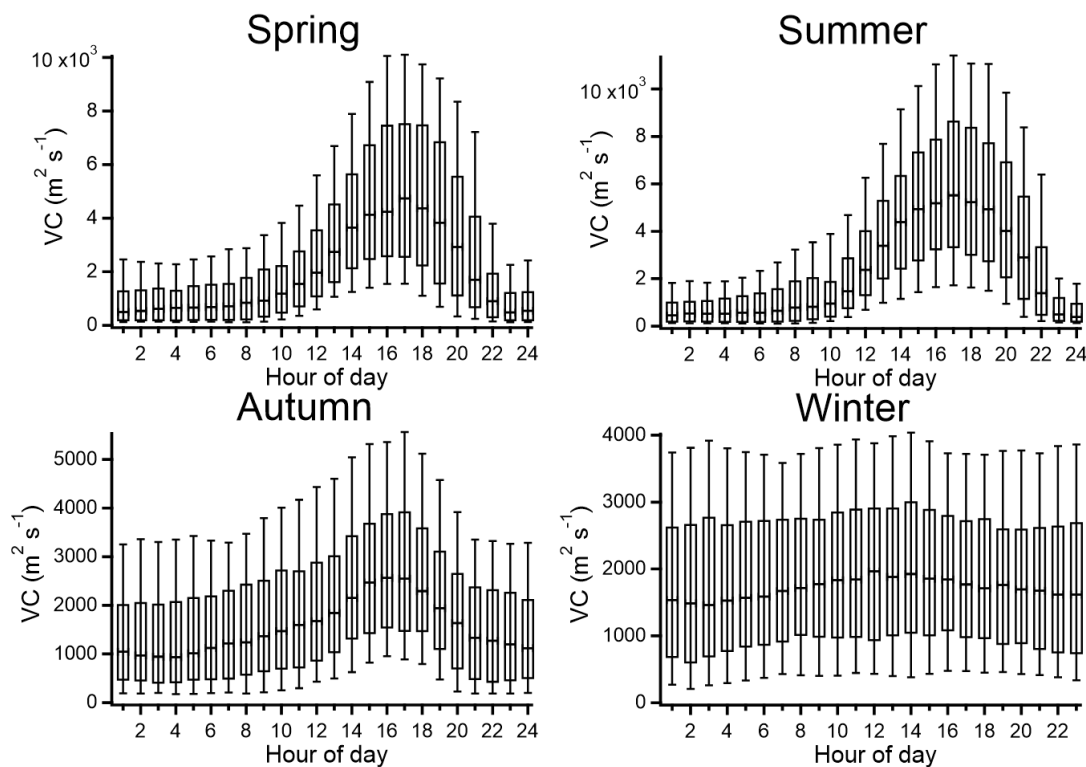
Figure S5: Total ACSM concentrations plus eBC measured by MAAP vs. PM_{2.5} measured by TEOM, coloured according to the sampling time. Slope coefficients and corresponding standard deviations were included.

23
24



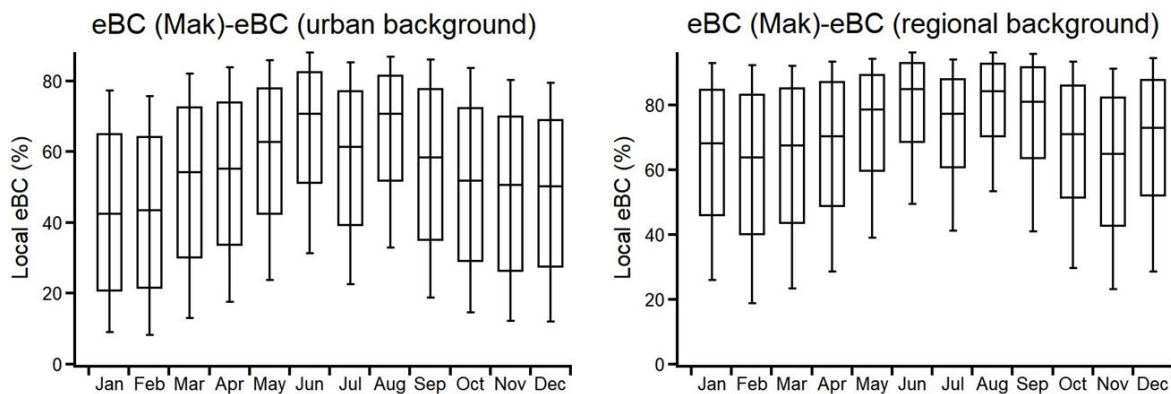
25

26 **Figure S6: PM₁ characterization determined by other studies performed over the globe in the last years**
 27 **(Green=organics; red=SO₄; blue=NO₃; yellow=NH₄; black=eBC).** The world map image was taken from Wikimedia
 28 commons (https://commons.wikimedia.org/wiki/File:World_map_blank_with_blue_sea.svg).
 29



30

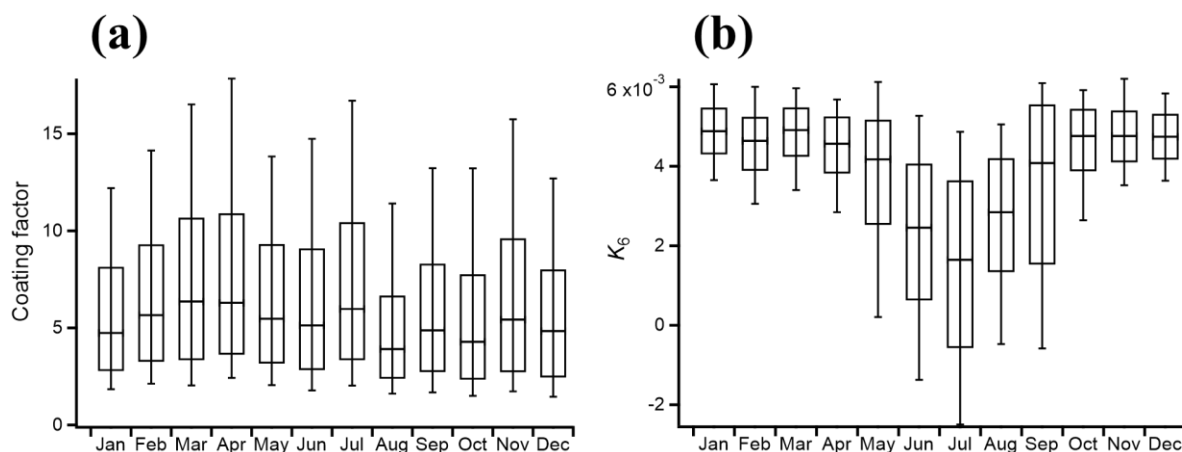
31 **Figure S7: Hourly variation of VC during the four seasons of the year.** Note the different scales of y-axis. In each box,
 32 the mid-line shows the median value for each x-value component, whisker bottom and top correspond to the 10th and
 33 90th percentiles, and box top and bottom correspond to 75th and 25th percentiles respectively.



34

35 **Figure S8: Monthly variation of local eBC at the sampling site. Local contribution of eBC was calculated by subtracting**
 36 **eBC measured at an urban background site (Kallio, left) and at a regional background site (Luukki, right) (Luoma et**
 37 **al., 2020) from the eBC measured at the street canyon site, and the remaining eBC was divided by the street canyon**
 38 **eBC concentration. In each box, the mid-line shows the median value for each x-value component, whisker bottom and**
 39 **top correspond to the 10th and 90th percentiles, and box top and bottom correspond to 75th and 25th percentiles**
 40 **respectively.**

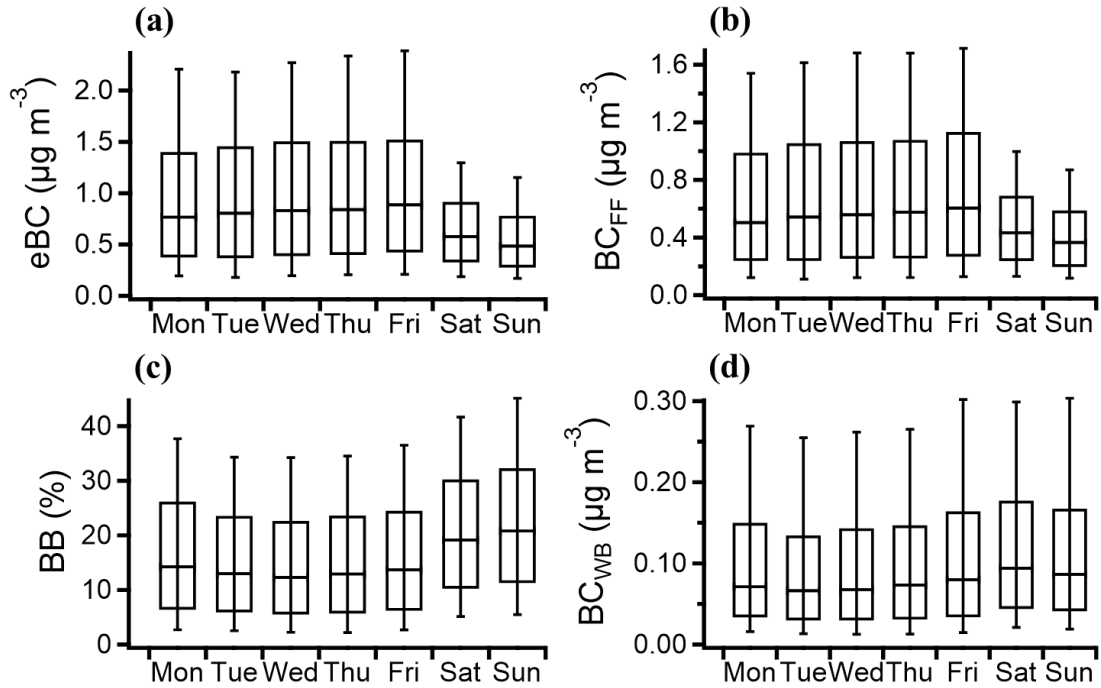
41



42

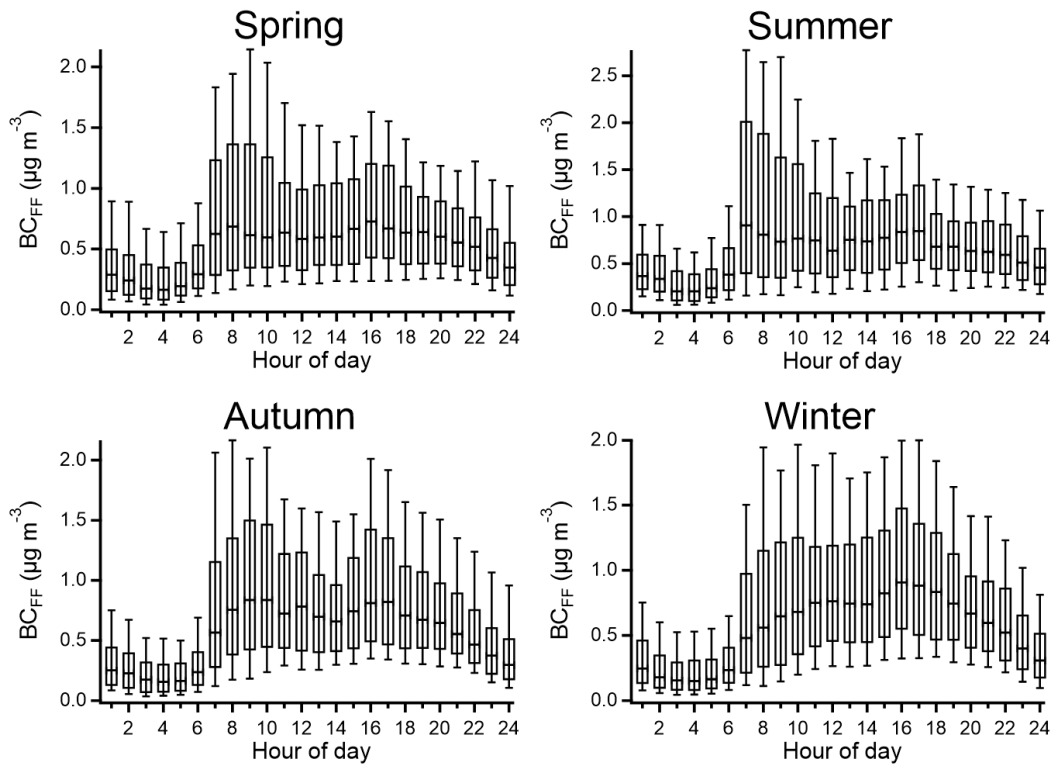
43 **Figure S9: Monthly variation of coating factor (a) and compensation parameter (K_6 , (b)). In each box, the mid-line**
 44 **shows the median value for each x-value component, whisker bottom and top correspond to the 10th and 90th percentiles,**
 45 **and box top and bottom correspond to 75th and 25th percentiles respectively.**

46



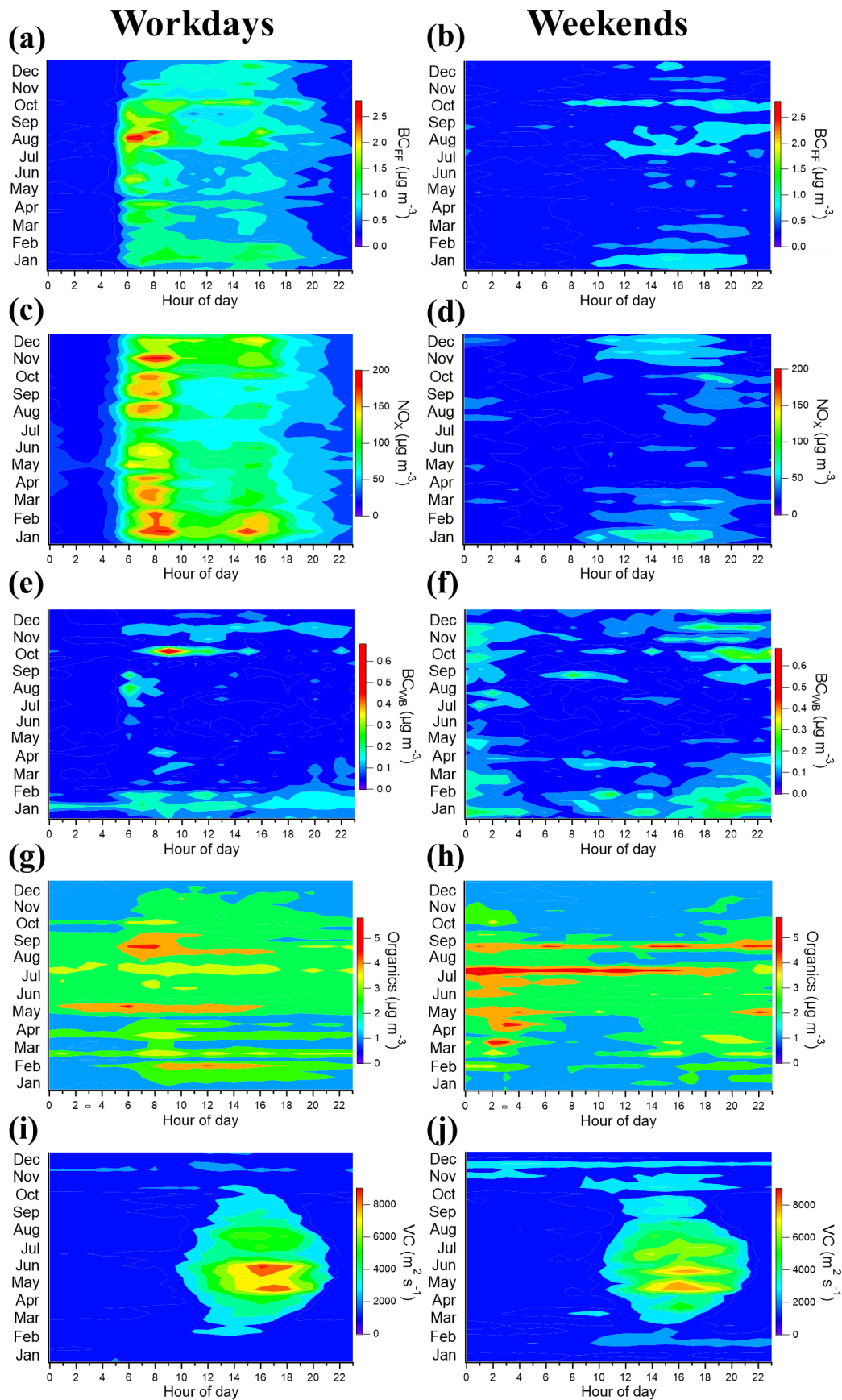
47

48 **Figure S10: Week variability of eBC (measured by MAAP), BC_{FF}, BB and BC_{WB} (determined by Aethalometer). In**
 49 **each box, the mid-line shows the median value for each x-value component, whisker bottom and top correspond to the**
 50 **10th and 90th percentiles, and box top and bottom correspond to 75th and 25th percentiles respectively.**
 51



52

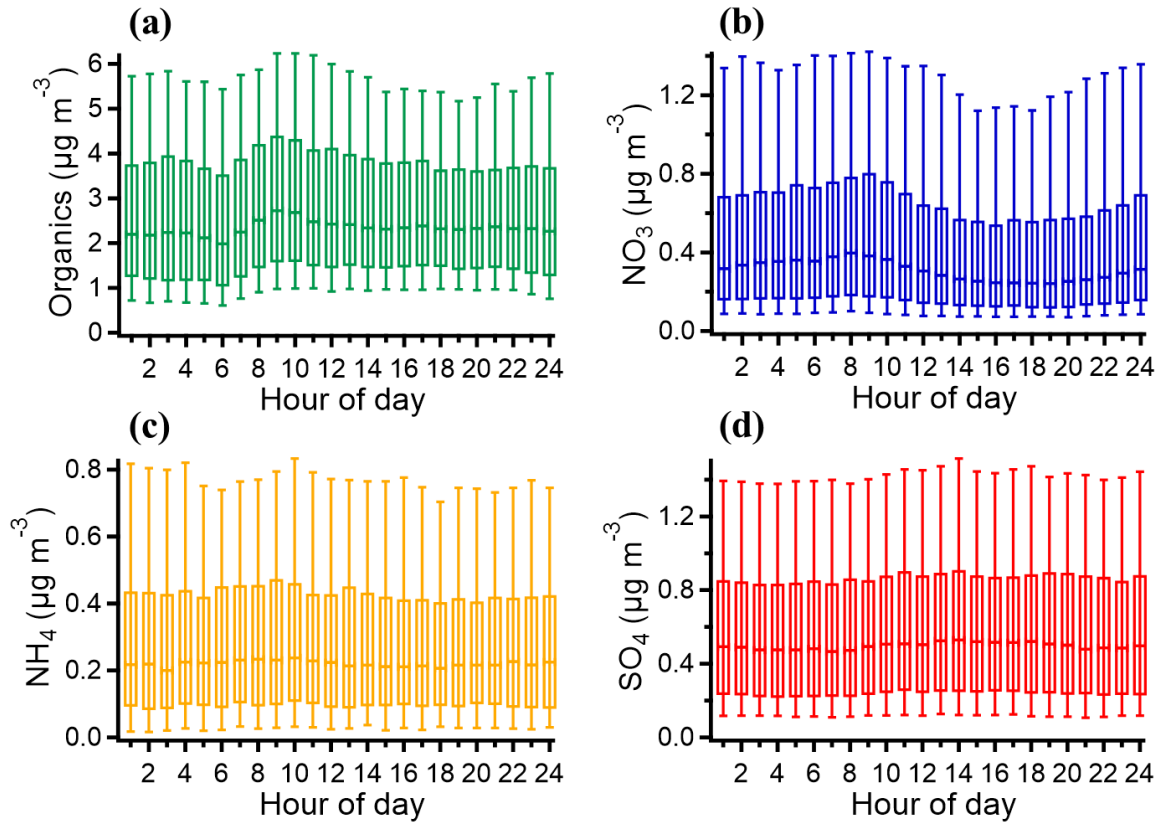
53 **Figure S11: Diurnal variation of BC_{FF} during the different seasons of the year (Spring, Summer, Autumn and Winter).**
 54 **In each box, the mid-line shows the median value for each x-value component, whisker bottom and top correspond to**
 55 **the 10th and 90th percentiles, and box top and bottom correspond to 75th and 25th percentiles respectively.**



56

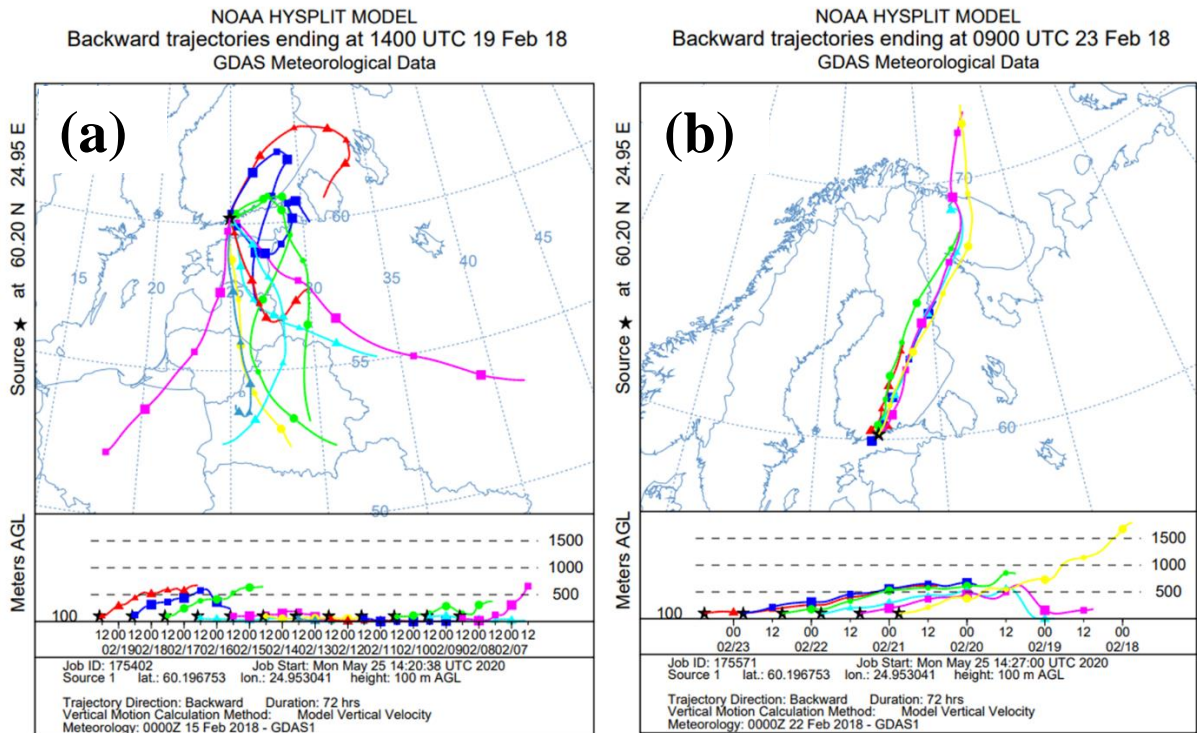
57
58

Figure S12: Diurnal and monthly variations of hourly median BC_{FF} , NO_x , BC_{WB} , organics and VC during workdays (left plots) and weekends (right plots).



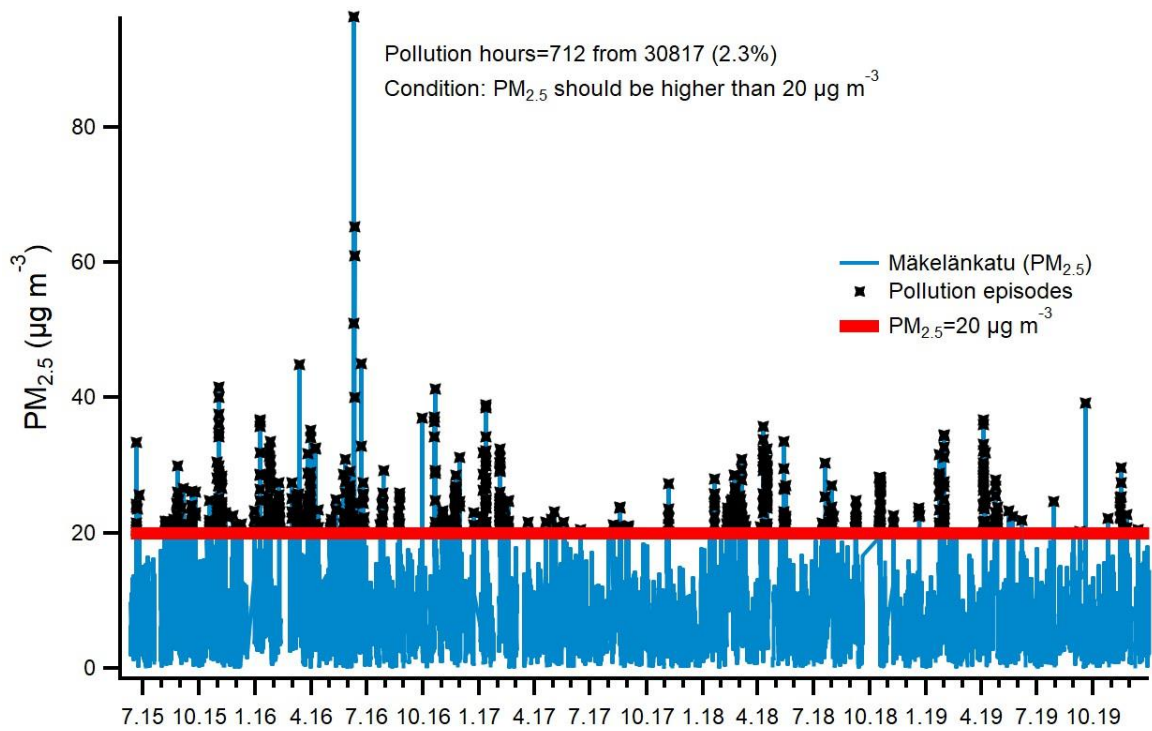
59

60 **Figure S13: Diurnal variation of NR-PM₁ constituents (Organics, NO₃, NH₄ and SO₄).** In each box, the mid-line shows
 61 the median value for each x-value component, whisker bottom and top correspond to the 10th and 90th percentiles, and
 62 box top and bottom correspond to 75th and 25th percentiles respectively.
 63



64

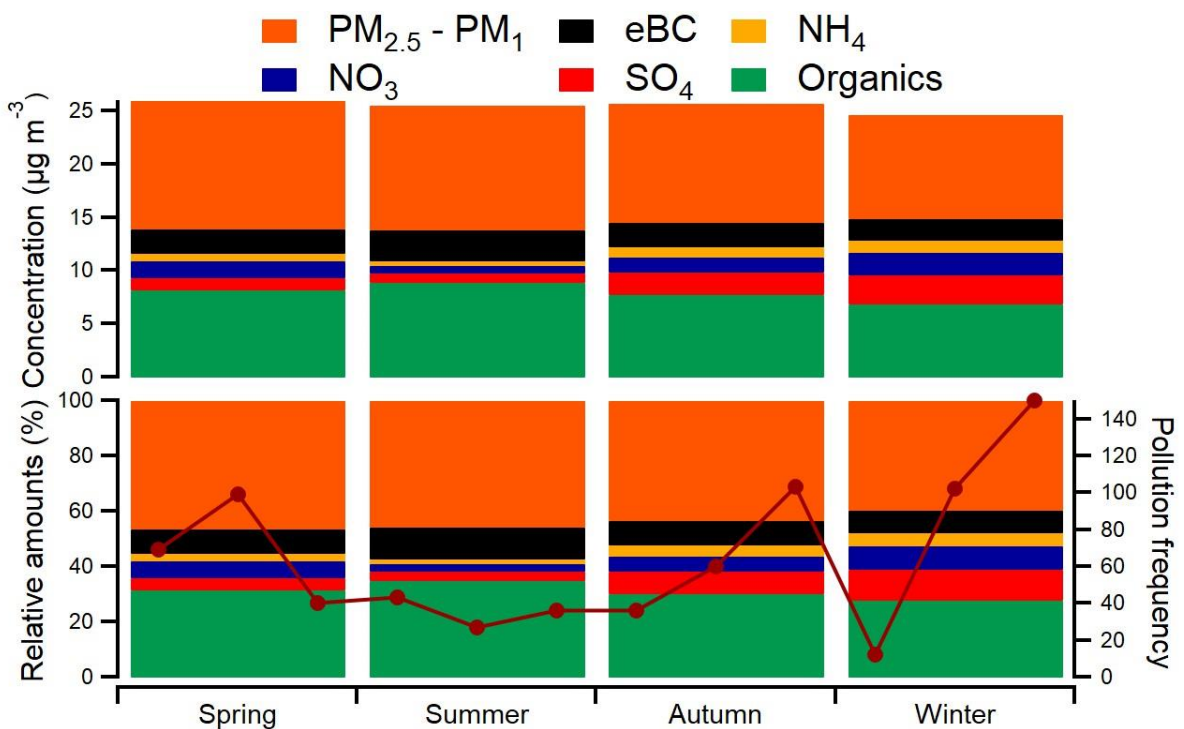
65 **Figure S14: Back trajectories observed during the measurement period for the long-range transport event (a) and for**
 66 **the local pollution event (b).**



67

68 Figure S15: Criteria used for evaluating the most intense pollution events occurring in Helsinki during the
 69 measurement period.

70



71

72 Figure S16: Seasonal variation in atmospheric aerosol particle constituent's median concentration and their
 73 corresponding relative amounts during the pollution episodes. The monthly pollution frequency was also included
 74 (brown line); Mar–May in spring, Jun–Aug in summer, Sep–Nov in autumn, and Dec–Feb in winter.

75

76 **S2 Meteorology at the Supersite station during the measurement period in 2015–2019**

77 The meteorological parameters measured during the period of 2015–2019 were evaluated to gain information on
78 the influence of local meteorological conditions on observed aerosol particle concentrations. The minimum
79 temperature was $-24.5\text{ }^{\circ}\text{C}$ (January 1st, 2016) and the maximum temperature was $+30.8\text{ }^{\circ}\text{C}$ (August 2nd, 2018).
80 The coldest month was January 2016 ($-8.6\text{ }^{\circ}\text{C}$), which was exceptionally cold. On the other hand, the warmest
81 month was July 2018 ($21.5\text{ }^{\circ}\text{C}$) that broke the earlier record of high monthly average temperature in Helsinki.
82 Generally, the coldest month in Helsinki is February with average temperature of $-7.0\text{ }^{\circ}\text{C}$ (1981–2010,
83 <https://www.ilmatieteenlaitos.fi/helmikuu>) and the warmest month is July with average temperature of $17.8\text{ }^{\circ}\text{C}$
84 (1981–2010, <https://www.ilmatieteenlaitos.fi/heinakuu>).

85 The relative humidity (RH) stayed mostly around 75–80 % during wintertime, while the driest periods
86 were observed in May with monthly average RH of 48–54 %. The values are close to what is commonly observed
87 in Helsinki. During the coldest seasons of the year, RH is usually about 90 %, while in spring and summer RH is
88 around 65 % (Pirinen et al., 2012). Wet deposition also influences significantly the measured atmospheric
89 concentrations by washing out the particles during precipitation events. During this study, the rainiest months
90 were between June to September, with maximum monthly precipitation sum observed in June 2016 (150,9 mm).
91 This result is in line with statistics from Helsinki between years 1981 and 2010, showing that the maximums of
92 monthly average rain accumulations are observed in August (80 mm) (<https://www.ilmatieteenlaitos.fi/elokuu>).

93 The maximum monthly average wind speeds were observed during winter with values between 5–5.5 m/s, while
94 summertime average wind speeds were between 3.4–4.5 m s^{-1} . Although the winds were stronger in wintertime,
95 the surface layer of atmosphere is usually more stable in wintertime than in summertime and mixing in vertical
96 direction is then more efficient during summer. The prevailing wind direction was south. The sampling site was
97 thus severely affected by pollutants transported from other regions of Europe.

98 The planetary boundary layer height (PBLH) had a strong seasonal variation, as expected in northern latitudes
99 where seasonality is particularly evident. The mixing height was relatively constant during wintertime, with the
100 median value of about 400 m. This value is consistent with stagnant conditions during this time of the year,
101 favoring the accumulation of PM in a relatively shallow boundary layer. On the other hand, summertime mixing-
102 heights had the lowest yearly values during night and early mornings (23h–10h) but increased rapidly up to above
103 2000 m during afternoon promoting dilution of atmospheric pollutants. The role of atmospheric dilution in
104 pollutant concentrations was evaluated by determining the ventilation coefficient ($\text{VC}=\text{wind speed} \times \text{PBLH}$), that
105 has been often used in other studies as a parameter to characterize pollutants dilution (e.g. Gani et al., 2019;
106 Sujatha et al., 2016). The VC dilution rate was much lower during the coldest periods of the year (Fig. S7),
107 contributing to increased amounts of PM. The highest VC during spring and summer coincides with an increase
108 in temperature and solar radiation that enhances convection and PBL growth.

109 **References**

- 110 Aurela, M., Saarikoski, S., Niemi, J. V., Canonaco, F., Prevot, A. S. H., Frey, A., Carbone, S., Kousa, A. and
 111 Hillamo, R.: Chemical and Source Characterization of Submicron Particles at Residential and Traffic Sites in the
 112 Helsinki Metropolitan Area, Finland, *Aerosol Air Qual. Res.*, 15(4), 1213–1226, doi:10.4209/aaqr.2014.11.0279,
 113 2015.
- 114 Carbone, S., Saarikoski, S., Frey, A., Reyes, F., Reyes, P., Castillo, M., Gramsch, E., Oyola, P., Jayne, J.,
 115 Worsnop, D. R. and others: Chemical characterization of submicron aerosol particles in Santiago de Chile,
 116 *Aerosol Air Qual. Res.*, 13(2), 462–473, doi:10.4209/aaqr.2012.10.0261, 2013.
- 117 Du, W., Sun, Y. L., Xu, Y. S., Jiang, Q., Wang, Q. Q., Yang, W., Wang, F., Bai, Z. P., Zhao, X. D. and Yang, Y.
 118 C.: Chemical characterization of submicron aerosol and particle growth events at a national background site (3295
 119 m a.s.l.) on the Tibetan Plateau, *Atmos. Chem. Phys.*, 15(18), 10811–10824, doi:10.5194/acp-15-10811-2015,
 120 2015.
- 121 Gani, S., Bhandari, S., Seraj, S., Wang, D. S., Patel, K., Soni, P., Arub, Z., Habib, G., Hildebrandt Ruiz, L. and
 122 Apte, J. S.: Submicron aerosol composition in the world's most polluted megacity: the Delhi Aerosol Supersite
 123 study, *Atmos. Chem. Phys.*, 19(10), 6843–6859, doi:10.5194/acp-19-6843-2019, 2019.
- 124 Gramsch, E., Reyes, F., Vásquez, Y., Oyola, P. and Rubio, M. A.: Prevalence of Freshly Generated Particles
 125 during Pollution Episodes in Santiago de Chile, *Aerosol Air Qual. Res.*, 16(9), 2172–2185,
 126 doi:10.4209/aaqr.2015.12.0691, 2016.
- 127 Hu, W., Hu, M., Hu, W.-W., Zheng, J., Chen, C., Wu, Y. and Guo, S.: Seasonal variations in high time-resolved
 128 chemical compositions, sources, and evolution of atmospheric submicron aerosols in the megacity Beijing, *Atmos.*
 129 *Chem. Phys.*, 17(16), 9979–10000, doi:10.5194/acp-17-9979-2017, 2017.
- 130 Jiang, Q., Wang, F. and Sun, Y.: Analysis of Chemical Composition, Source and Processing Characteristics of
 131 Submicron Aerosol during the Summer in Beijing, China, *Aerosol Air Qual. Res.*, 19(6), 1450–1462,
 132 doi:10.4209/aaqr.2018.12.0480, 2019.
- 133 Katsanos, D., Bougiatioti, A., Liakakou, E., Kaskaoutis, D. G., Stavroulas, I., Paraskevopoulou, D., Lianou, M.,
 134 Psiloglou, B. E., Gerasopoulos, E., Pilinis, C. and Mihalopoulos, N.: Optical Properties of Near-Surface Urban
 135 Aerosols and their Chemical Tracing in a Mediterranean City (Athens), *Aerosol Air Qual. Res.*, 19(1), 49–70,
 136 doi:10.4209/aaqr.2017.11.0544, 2019.
- 137 Levy, M. E., Zhang, R., Zheng, J., Tan, H., Wang, Y., Molina, L. T., Takahama, S., Russell, L. M. and Li, G.:
 138 Measurements of submicron aerosols at the California–Mexico border during the Cal–Mex 2010 field campaign,
 139 *Atmos. Environ.*, 88, 308–319, doi:10.1016/j.atmosenv.2013.08.062, 2014.
- 140 Lin, C., Ceburnis, D., Huang, R.-J., Xu, W., Spohn, T., Martin, D., Buckley, P., Wenger, J., Hellebust, S., Rinaldi,
 141 M., Facchini, M. C., O'Dowd, C. and Ovadnevaite, J.: Wintertime aerosol dominated by solid-fuel-burning
 142 emissions across Ireland: insight into the spatial and chemical variation in submicron aerosol, *Atmos. Chem.*
 143 *Phys.*, 19(22), 14091–14106, doi: 10.5194/acp-19-14091-2019, 2019.
- 144 Minguillón, M. C., Ripoll, A., Pérez, N., Prévôt, A. S. H., Canonaco, F., Querol, X. and Alastuey, A.: Chemical
 145 characterization of submicron regional background aerosols in the western Mediterranean using an Aerosol
 146 Chemical Speciation Monitor, *Atmos. Chem. Phys.*, 15(11), 6379–6391, doi:10.5194/acp-15-6379-2015, 2015.
- 147 Pirinen, P., Simola, H., Aalto, J., Kaukoranta, J. P., Karlsson, P. and Ruuhela, R.: Statistics on the Finnish climate
 148 1981-2010, Finnish Meteorological Institute, 2012.
- 149 Qin, Y. M., Tan, H. B., Li, Y. J., Schurman, M. I., Li, F., Canonaco, F., Prévôt, A. S. H. and Chan, C. K.: Impacts
 150 of traffic emissions on atmospheric particulate nitrate and organics at a downwind site on the periphery of
 151 Guangzhou, China, *Atmos. Chem. Phys.*, 17(17), 10245–10258, doi:10.5194/acp-17-10245-2017, 2017.
- 152 Ripoll, A., Minguillón, M. C., Pey, J., Jimenez, J. L., Day, D. A., Sosedova, Y., Canonaco, F., Prévôt, A. S. H.,
 153 Querol, X. and Alastuey, A.: Long-term real-time chemical characterization of submicron aerosols at Montsec
 154 (southern Pyrenees, 1570 m a.s.l.), *Atmos. Chem. Phys.*, 15(6), 2935–2951, doi:10.5194/acp-15-2935-2015, 2015.

- 155 Salcedo, D., Alvarez-Ospina, H., Peralta, O. and Castro, T.: PM₁ Chemical Characterization during the ACU15
156 Campaign, South of Mexico City, *Atmosphere*, 9(6), 232, doi:10.3390/atmos9060232, 2018.
- 157 Schlag, P., Kiendler-Scharr, A., Blom, M. J., Canonaco, F., Henzing, J. S., Moerman, M., Prévôt, A. S. H. and
158 Holzinger, R.: Aerosol source apportionment from 1-year measurements at the CESAR tower in Cabauw, the
159 Netherlands, *Atmos. Chem. Phys.*, 16(14), 8831–8847, doi:10.5194/acp-16-8831-2016, 2016.
- 160 Sujatha, P., Mahalakshmi, D. V., Ramiz, A., Rao, P. V. N. and Naidu, C. V.: Ventilation coefficient and boundary
161 layer height impact on urban air quality, edited by Z. Wang, *Cogent Environ. Sci.*, 2(1),
162 doi:10.1080/23311843.2015.1125284, 2016.
- 163 Sun, Y.-L., Zhang, Q., Schwab, J. J., Demerjian, K. L., Chen, W.-N., Bae, M.-S., Hung, H.-M., Hogrefe, O.,
164 Frank, B., Rattigan, O. V. and Lin, Y.-C.: Characterization of the sources and processes of organic and inorganic
165 aerosols in New York city with a high-resolution time-of-flight aerosol mass spectrometer, *Atmos. Chem. Phys.*,
166 11(4), 1581–1602, doi:10.5194/acp-11-1581-2011, 2011.
- 167 Teinilä, K., Aurela, M., Niemi, J. V., Kousa, A., Petäjä, T., Järvi, L., Hillamo, R., Kangas, L., Saarikoski, S. and
168 Timonen, H.: Concentration variation of gaseous and particulate pollutants in the Helsinki city centre —
169 observations from a two-year campaign from 2013–2015, *Boreal Env. Res.*, 24, 22, 2019.
- 170 Tiitta, P., Vakkari, V., Croteau, P., Beukes, J. P., van Zyl, P. G., Josipovic, M., Venter, A. D., Jaars, K., Pienaar,
171 J. J., Ng, N. L., Canagaratna, M. R., Jayne, J. T., Kerminen, V.-M., Kokkola, H., Kulmala, M., Laaksonen, A.,
172 Worsnop, D. R. and Laakso, L.: Chemical composition, main sources and temporal variability of PM₁ aerosols
173 in southern African grassland, *Atmos. Chem. Phys.*, 14(4), 1909–1927, doi:10.5194/acp-14-1909-2014, 2014.
- 174 Xu, W., Sun, Y., Wang, Q., Zhao, J., Wang, J., Ge, X., Xie, C., Zhou, W., Du, W., Li, J., Fu, P., Wang, Z.,
175 Worsnop, D. R. and Coe, H.: Changes in Aerosol Chemistry From 2014 to 2016 in Winter in Beijing: Insights
176 From High-Resolution Aerosol Mass Spectrometry, *J. Geophys. Res. Atmos.*, 124(2), 1132–1147,
177 doi:10.1029/2018JD029245, 2019.
- 178 Young, D. E., Kim, H., Parworth, C., Zhou, S., Zhang, X., Cappa, C. D., Seco, R., Kim, S. and Zhang, Q.:
179 Influences of emission sources and meteorology on aerosol chemistry in a polluted urban environment: results
180 from DISCOVER-AQ California, *Atmos. Chem. Phys.*, 16(8), 5427–5451, doi:10.5194/acp-16-5427-2016, 2016.
- 181 Zhang, Y., Favez, O., Petit, J.-E., Canonaco, F., Truong, F., Bonnaire, N., Crenn, V., Amodeo, T., Prévôt, A. S.
182 H., Sciare, J., Gros, V. and Albinet, A.: Six-year source apportionment of submicron organic aerosols from near-
183 continuous highly time-resolved measurements at SIRTa (Paris area, France), *Atmos. Chem. Phys.*, 19(23),
184 14755–14776, doi: 10.5194/acp-19-14755-2019, 2019.